The Astrophysical Journal Letters, 936:L3 (6pp), 2022 September 1 https://doi.org/10.3847/2041-8213/ac86d3

Antaeus: A Retrograde Group of Tidal Debris in the Milky Way's Disk Plane

Pierre-Antoine Oria[1], Wassim Tenachi[1], Rodrigo Ibata[1], Benoit Famaey[1], Zhen Yuan[1], Anke Arentsen[1], Nicolas Martin[1], and Akshara Viswanathan[2]
[1] Université de Strasbourg, CNRS, Observatoire astronomique de Strasbourg, UMR 7550, F-67000 Strasbourg, France; pierre-antoine.oria@astro.unistra.fr
[2] Kapteyn Astronomical Institute, University of Groningen, Landleven 12, NL-9747AD Groningen, The Netherlands
Received 2022 June 21; revised 2022 August 1; accepted 2022 August 1; published 2022 August 26

Abstract

We present the discovery of a wide retrograde moving group in the disk plane of the Milky Way using action-angle coordinates derived from the Gaia DR3 catalog. The structure is identified from a sample of its members that are currently almost at the pericenter of their orbit and are passing through the solar neighborhood. The motions of the stars in this group are highly correlated, indicating that the system is probably not phase mixed. With a width of at least 1.5 kpc and with a probable intrinsic spread in metallicity, this structure is most likely the wide remnant of a tidal stream of a disrupted ancient dwarf galaxy (age $\sim$12 Gyr, $\langle[\mathrm{Fe/H}]\rangle \sim -1.74$). The structure presents many similarities (e.g., in energy, angular momentum, metallicity, and eccentricity) with the Sequoia merging event. However, it possesses extremely low vertical action J_z, which makes it unique even among Sequoia dynamical groups. As the low J_z may be attributable to dynamical friction, we speculate that these stars may be the remnants of the dense core of the Sequoia progenitor.

Unified Astronomy Thesaurus concepts: Galaxies (573); Stellar streams (2166); Milky Way dynamics (1051); Local Group (929); Milky Way stellar halo (1060); Tidal disruption (1696); Milky Way disk (1050)

Supporting material: machine-readable table

1. Introduction

The complex formation and merging history of the Milky Way (MW) can perhaps be best understood by examining its stellar halo, host to many tidal debris of disrupted galaxies and globular clusters. Dynamical times in the halo are long, so the debris can persist there as coherent phase-space structures for billions of years (see, e.g., Helmi & de Zeeuw 2000), making them easier for us to detect.

With the advent of the Gaia mission (Gaia Collaboration et al. 2016) and its superb astrometric data, the task of digging into the stellar halo to uncover the past has been made more accessible. The stellar halo of the MW is now understood to be the product of several important accretion events making up most of its population (Di Matteo et al. 2019), the biggest of which is Gaia–Sausage/Enceladus (Belokurov et al. 2018; Helmi et al. 2018). Stream-finding algorithms (Malhan et al. 2018; Ibata et al. 2021) have now detected dozens of kinematically coherent structures that will help to chart the acceleration field of our galaxy, providing a wealth of model-agnostic information.

The Gaia data also make it possible to use action coordinates (J_r, J_ϕ, and J_z) to detect stellar structures. Actions keep relevance over very long times if the potential evolves slowly and are thus especially useful to trace past mergers. Recently, Yuan et al. (2020), Naidu et al. (2020), and Malhan et al. (2022) used these quantities to detect and construct maps of the MW's dynamical groups and to link them to important merger events.

A similar technique was employed by Myeong et al. (2018) to find several retrograde structures in the stellar halo that were then tentatively associated with the ω Centauri globular cluster, which Majewski et al. (2012) had already suspected of bringing in such material. Retrograde structures have been linked to accretion events for a long time (Carollo et al. 2007), and it has been confirmed by Helmi et al. (2017) that the less bound stars in the halo are typically on retrograde orbits. Sestito et al. (2021) also highlight the importance of the metal-poor retrograde halo population for tracing the early building blocks of the galaxy.

Myeong et al. (2019) reexamined the structures from Myeong et al. (2018) and linked them to a substantial merger event that they named Sequoia. The Sequoia progenitor galaxy could have brought those retrograde groups and possibly the ω Centauri as well. The fact that its stellar population is distinct in metallicity and orbital parameters from the Gaia–Sausage makes the event another important piece of the stellar halo puzzle.

In this work we present the discovery of Antaeus,[3] a retrograde high-energy group of tidal debris in the MW's disk plane, made using action-angle coordinates derived from the Gaia DR3 catalog (Gaia Collaboration 2022) and the Stäckel fudge implemented in AGAMA (Vasiliev 2019). The new structure has several properties that are similar to those of Sequoia stars, so we discuss its possible affiliation to this event, although both its position in the disk of the MW and its extraordinary low vertical action make it stand out.

2. Selection process

Throughout this Letter, we use the right-hand side Galactic Cartesian coordinates for the MW with the Sun located at $(x, y, z)_\odot = (-8.2240, 0, 0.0028)$ kpc (taking the solar radius from Bovy 2020 and the height above the midplane from Widmark et al. 2021) having the peculiar velocity $(v_x, v_y, v_z)_\odot = (11.10, 7.20, 7.25)$ km s^{-1} (Schönrich et al. 2010, but

[3] In Greek mythology, Antaeus is the child of Gaia and Poseidon, a giant whose name comes from "opponent."

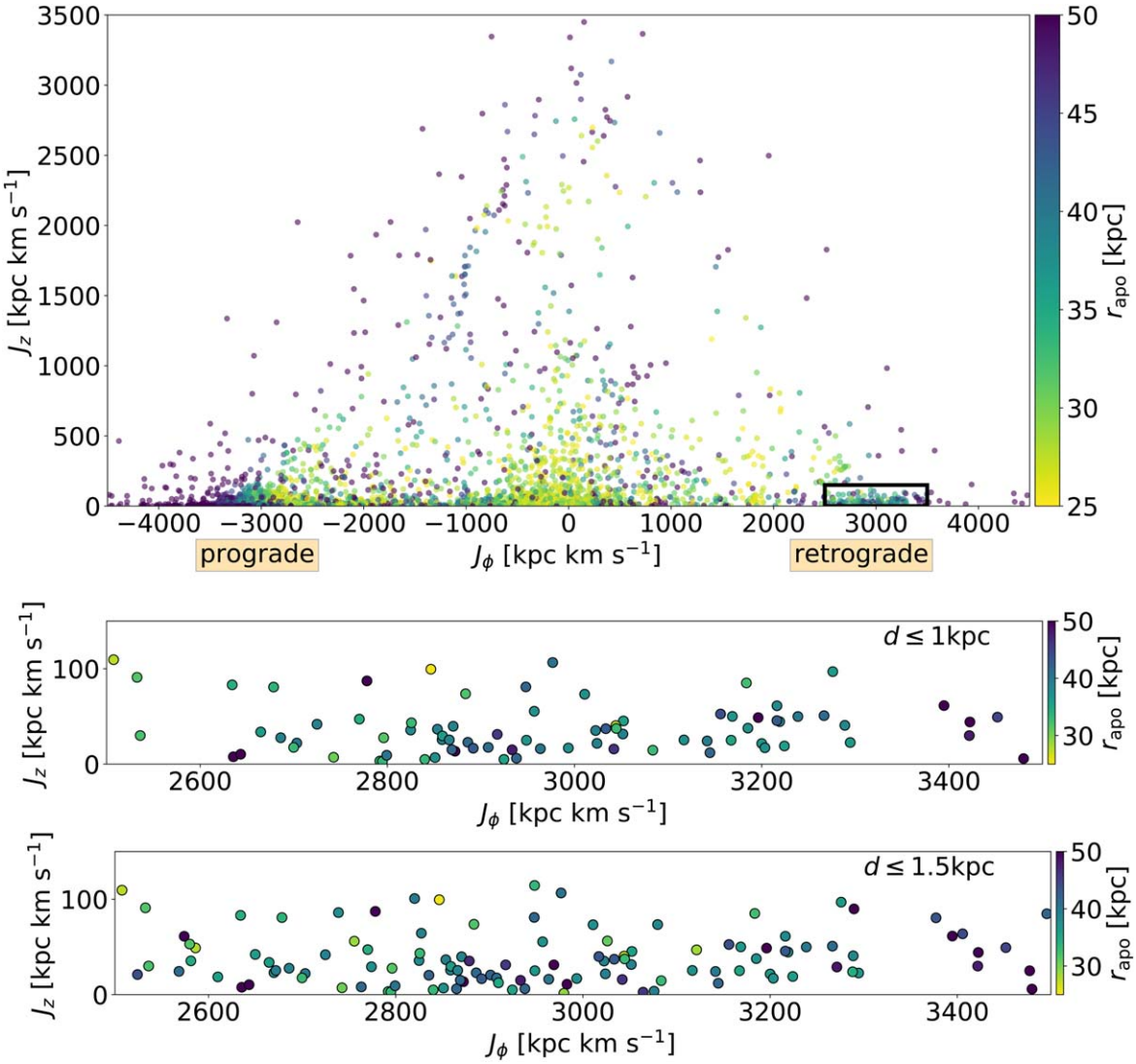

Figure 1. Selection procedure. Top panel: Gaia DR3 stars from the selection process described in Section 2 (i.e., $\varpi/\delta\varpi > 10$, $r_{apo} \geqslant 25$ kpc, and $d \leqslant 1.5$ kpc). Middle panel: zoom on the low J_z region delimited by the rectangle in the top panel ($2500 \leqslant J_\phi \leqslant 3500$ km s^{-1} kpc, $J_z \leqslant 150$ km s^{-1} kpc). Bottom panel: same region as the middle panel, but for our final cut using distances $d \leqslant 1$ kpc from the Sun.

Table 1
Sample from the 80 Stars of Our Selection from Section 2

Gaia Source ID	R.A. (deg)	Decl. (deg)	J_r (kpc km s^{-1})	J_z (kpc km s^{-1})	J_ϕ (kpc km s^{-1})	r_{peri} (kpc)	r_{apo} (kpc)	e	(Fe/H) (dex)
3857834273536171808	159.91	4.08	1843.09	106.55	2976.68	7.31	40.78	0.70	-2.09 ± 0.30
1558668134509319040	204.99	49.77	698.65	99.50	2846.51	8.19	25.57	0.51	-1.97 ± 0.12
1374889335770878848	232.59	35.38	1936.15	45.67	3216.25	7.72	43.03	0.70	-1.88 ± 0.10
9506369673976295 68	102.78	40.33	1505.39	83.11	2634.22	6.55	34.23	0.68	-1.77 ± 0.13
3839165510915273856	139.71	−0.89	1963.65	80.95	2947.99	7.09	41.87	0.71	-1.76 ± 0.08
2657496656325125888	347.59	1.19	1963.74	9.28	2799.33	6.41	40.27	0.73	-1.62 ± 0.12
231238462236707584	57.75	42.07	1680.13	33.76	2664.73	6.34	36.15	0.70	-1.54 ± 0.08
3834229356541509760	147.87	0.89	1466.15	47.20	2770.15	6.84	34.32	0.67	-1.33 ± 0.23
1950571427690143616	322.99	34.92	1216.32	14.63	3083.68	7.90	32.92	0.61	...
2340952515729081728	359.75	−21.81	1340.28	91.00	2532.56	6.35	31.65	0.67	...

Note. The information is derived from the MW potential of McMillan (2017).

(This table is available in its entirety in machine-readable form.)

with the velocity in the direction of Galactic rotation taken from Bovy 2020), and circular velocity $v_c(R = R_\odot) = 243$ km s^{-1} (Bovy 2020). Our starting point is the Radial Velocity Spectrometer (RVS; Recio-Blanco et al. 2022) sample of Gaia DR3, for which we derive action-angle coordinates (J_r, J_ϕ, and J_z) and orbital parameters using AGAMA (Vasiliev 2019) in the

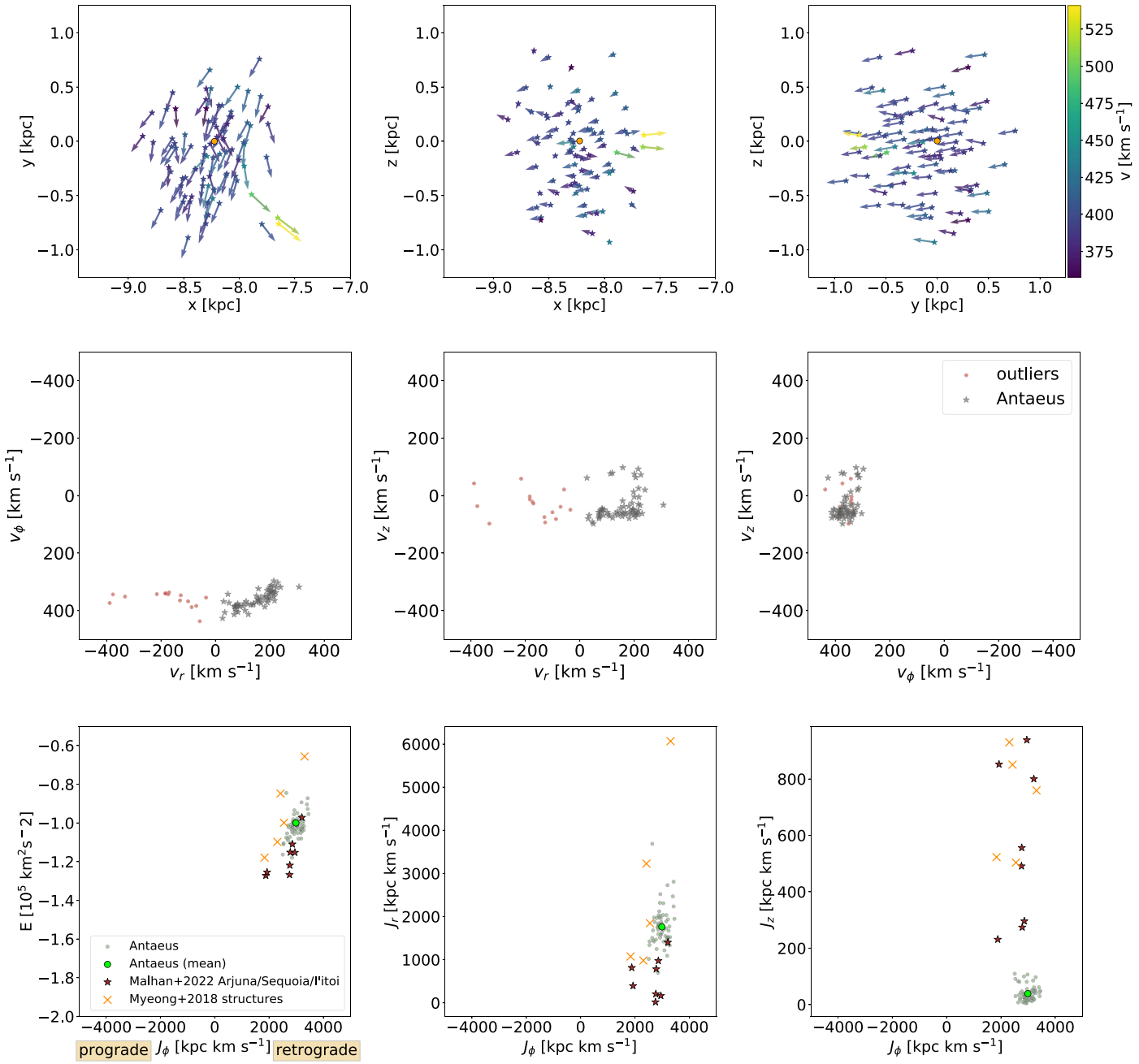

Figure 2. Top panel: position and velocity vectors of our selection of stars from Section 2 colored by total velocity; we plot bulk motion outliers with a slightly transparent line. The orange ball represents the Sun. Antaeus stars are currently passing through our solar neighborhood, going in a retrograde motion in the MW's disk plane. Middle panel: velocity planes $v_r v_\phi$, $v_r v_z$, and $v_\phi v_z$ with the outliers (red dots) from the top panel bulk motion separated from Antaeus' stars (black). Note that we inverted the v_ϕ axes to be coherent with usual velocity plots. Bottom panel: position of Antaeus (green dots) in energy E and actions J_r, J_ϕ, and J_z, compared to Sequoia-associated retrograde structures from Myeong et al. (2018; orange crosses) and Arjuna/Sequoia/I'itoi-associated streams and globular clusters from Malhan et al. (2022; brown stars).

MW gravitational potential of McMillan (2017). From this catalog, we take the stars with good parallax measurements ($\varpi/\delta\varpi \geqslant 10$) and $d \leqslant 1.5$ kpc so as to retain a good quality solar neighborhood sample. Since our aim is to investigate the structures that are falling down onto the MW, we choose to select stars with large apocenter distances, $r_{\rm apo} \geqslant 25$ kpc. These cuts leave us with 3624 stars; we plot the resulting selection in the $J_\phi J_z$ plane, colored by $r_{\rm apo}$, in Figure 1 (top panel).

Among the many interesting structures that stand out from this view, we focus our attention on the low J_z, retrograde moving group of stars delimited by the black rectangle ($2500 \leqslant J_\phi \leqslant 3500$ km s^{-1} kpc, $J_z \leqslant 150$ km s^{-1} kpc), into which we zoom in Figure 1 (middle panel). We notice a good agreement in apocenters for stars in this region, further suggesting the presence of a stellar structure with coherent motion.

Finally, we experimented with the heliocentric distance cut to see how the selection changes. We noticed that by selecting stars within a distance of $d \leqslant 1$ kpc from the Sun (Figure 1, bottom panel) the agreement in apocenters is slightly better, removing in particular some extreme values from the previous cut. This leaves a sample of 80 stars, which are listed in Table 1.

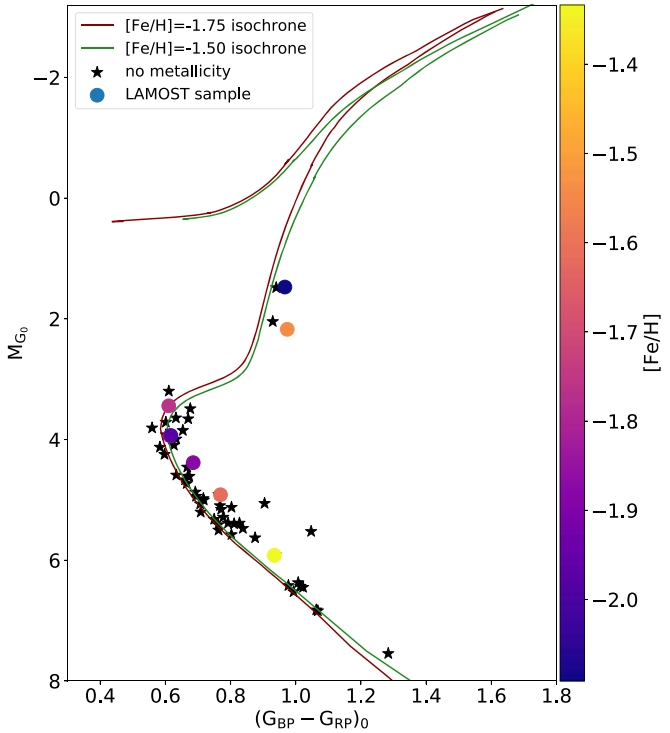

Figure 3. Color–magnitude diagram for our sample of Antaeus stars, compared to PARSEC model isochrones (Bressan et al. 2012) of age 12 Gyr and metallicities [Fe/H] = −1.75 (red) and [Fe/H] = −1.50 (green). The colorbar gives the [Fe/H] for the eight LAMOST stars.

In order to establish the statistical significance of this detection, we repeat the same selection on the Gaia Universe Model Snapshot (GUMS; Robin et al. (2012) simulation updated for DR3. The initial $d \leqslant 1.5$ kpc cut on GUMS gives 3781 stars, very close to the number of stars in our DR3 selection. Normalizing for this small difference, we find that there is, in the final selection (black rectangle in Figure 1), more than 5 times the number of stars in DR3 than there is in GUMS. Furthermore, the distribution along the J_ϕ axis is bimodal in the GUMS data, with a main peak in the prograde region ($J_\phi \approx -3000$) and a small peak around $J_\phi = 0$, while the same distribution in our DR3 selection is trimodal with an additional peak in the retrograde region ($J_\phi \approx 3000$) corresponding to Antaeus, and the peak around $J_\phi = 0$ being more pronounced. Using the GUMS simulation as an estimate of the expected Galactic populations, the Antaeus feature corresponds to a $\approx 7\sigma$ detection.

3. Sample Characteristics

We show the positions and the velocities of our selection of stars in Figure 2 (top panel). It appears clear that the stars belong to a coherent structure dynamically, moving in a retrograde motion in the disk plane of the MW. The structure is rather thick, with a width of at least 1.5 kpc. We identify some outliers from this bulk motion, which all have a distinctive positive velocity in the x direction ($v_x \geqslant 0$). For the remainder of this study, we will exclude those 15 outliers from our sample, leaving us with 65 stars of the Antaeus stream. In Figure 2 (middle panel), we plot velocity planes $v_r v_\phi$, $v_r v_z$, and $v_\phi v_z$ with this separation taken into account, showing the compactness of Antaeus stars in those projections.

We crossmatch our selection with the LAMOST DR8 catalog (Wang et al. 2022) and find eight stars in common, for which we obtain metallicities from their "FEH_PASTEL" values. These LAMOST stars have a mean of $[\mathrm{Fe/H}] = -1.74^{+0.06}_{-0.07}$, with an intrinsic spread of $\sigma = 0.11^{+0.10}_{-0.04}$ (correcting for the LAMOST metallicity uncertainty estimates) and individual values ranging from $[\mathrm{Fe/H}] = -1.33 \pm 0.23$ to $[\mathrm{Fe/H}] = -2.09 \pm 0.30$. The color–magnitude diagram (CMD) of the sample is shown in Figure 3, compared to old metal-poor isochrones (12 Gyr, [Fe/H] = −1.75, and [Fe/H] = −1.50) from the PARSEC library (Bressan et al. 2012). The photometry is corrected for interstellar extinction using the 3D extinction estimates calculated by Anders et al. (2022).

Finally, we integrate back in time the orbits of the Antaeus stars in the McMillan MW potential for 1.5 Gyr, and in the MWPotential2014 (Bovy 2015); we show the results in Figure 4. Here also the structure appears very coherent dynamically. We find, for the McMillan MW potential ($M_{\rm vir} = 1.3 \times 10^{12}\, M_\odot$), a mean pericenter radius of $r_{\rm peri} = 7.3$ kpc, a mean apocenter radius of $r_{\rm apo} = 39.3$ kpc, a mean orbital eccentricity of $e = 0.69$, and a mean orbital time of $t_{\rm orbit} = 1.1$ Gyr. For the lighter MWPotential2014, however ($M_{\rm vir} = 8 \times 10^{11}\, M_\odot$), those values become a mean of $r_{\rm peri} = 7.3$ kpc, a mean of $r_{\rm apo} = 71.9$ kpc, a mean of $e = 0.81$, and a mean of $t_{\rm orbit} = 1.5$ Gyr. The eight LAMOST stars, whose orbits are plotted in solid black, appear to be good representative members of the stream.

The mean actions of stars in the structure are ($J_r = 1761$, $J_\phi = 2990$, $J_z = 39$) kpc km s^{-1}, and their mean energy is $E = -10^5$ km^2 s^{-2} (in the McMillan 2017 potential model); we show this information for individual stars in Figure 2 (bottom panel).

4. Discussion and Conclusions

Based on the characteristics derived in Section 3, in particular the thickness of the structure (width $\simeq$1.5 kpc) and the range of metallicity of its constituent stars, it seems highly likely that this group of stars is the remnant of a tidal stream of a disrupted dwarf galaxy. The CMD (Figure 3) seems to indicate that the progenitor is seemingly very old, probably around ∼12 Gyr in age. The agreement is better with a model metallicity of [Fe/H] = −1.50, although we derive a mean value of $[\mathrm{Fe/H}] = -1.74^{+0.06}_{-0.07}$. It would thus be very helpful to extend our sample of metallicities to help decide the matter. Such metallicities give an estimated stellar mass of 10^6–$10^7\, M_\odot$ according to the $z = 0$ mass–metallicity relation of Kirby et al. (2013). Taking into account the redshift evolution of such relations (for a given metallicity, higher mass at higher redshift is required), we can consider that those constitute lower bounds and that the progenitor probably has a rather high stellar mass of $\geqslant 10^7\, M_\odot$, making it likely that it is linked to an already known accretion event.

Indeed, when comparing with known halo structures, we find that the mean J_ϕ, energy, and eccentricities of our sample of Antaeus stars show many similarities with the Arjuna/I'itoi/Sequoia group of mergers (Naidu et al. 2020). However, Antaeus seems more akin to the retrograde structures of Myeong et al. (2018) and to the retrograde tail of the Sequoia event (Myeong et al. 2019; see the bottom row in Figure 2 for a comparison to the previously mentioned groups), especially when factoring in the metallicity of its population. The ∼12 Gyr age derived from the CMD comparison is also consistent with estimates for Sequoia groups (Ruiz-Lara et al. 2022).

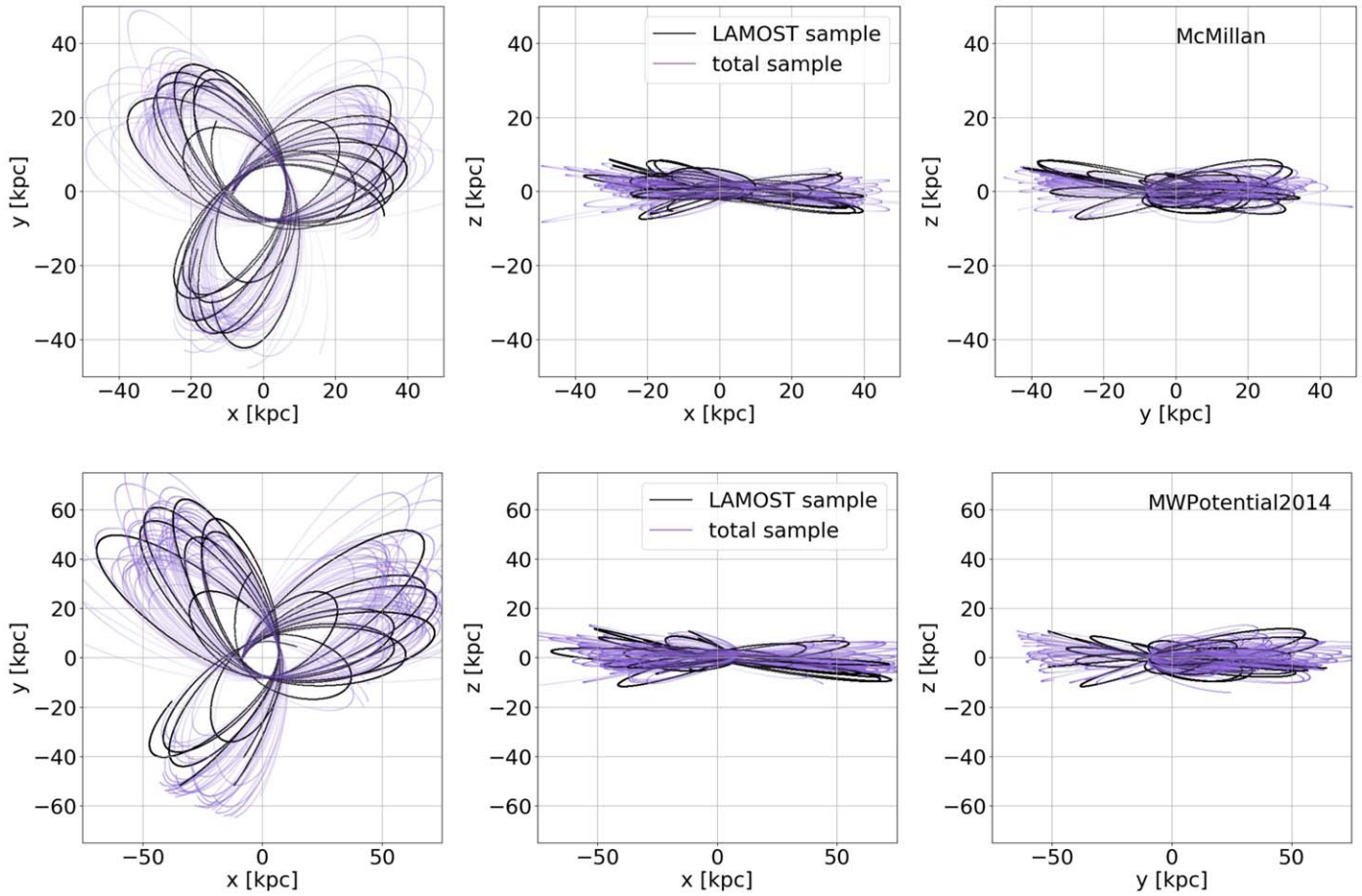

Figure 4. Orbits of Antaeus stars seen in Galactic Cartesian coordinates, integrated backwards in the McMillan (2017) MW potential for 1.5 Gyr (top panel), and in the MWPotential2014 model for 2.5 Gyr (bottom panel). Notice the change of scales, as stars go farther when integrated in the lighter MWPotential2014. Orbits of the LAMOST sample (eight stars) are in solid black, and orbits of the rest of our sample (57 stars) are in purple.

Nonetheless, Antaeus' extraordinarily low mean J_z and its position in the disk plane of the MW both make it unique, even when compared to the global atlas of halo structures from Malhan et al. (2022). It may be the distinct, low J_z tail of the L-RL64 cluster discovered by Ruiz-Lara et al. (2022) and also detected by Dodd et al. (2022). If the structure is indeed related to Sequoia, this difference has to be explained.

The mere existence of such a streamy, retrograde structure in the disk of the MW is very puzzling. It is not clear how such kinematic coherence could be retained if this population came in with Sequoia $9 \sim 11$ Gyr ago (Myeong et al. 2019). Of course Antaeus' progenitor could have arrived initially with a small inclination, although this possibility appears somewhat contrived. See, however, the simulations from Amarante et al. (2022) in which nearly radial mergers could potentially produce such populations. It seems more natural to explain the very low quantity of vertical motion by dissipation due to dynamical friction, which might be consistent with an early arrival in the MW. This scenario would invite the possibility that Antaeus is the debris of the dense core of the Sequoia progenitor, which would have stabilized in the disk through dynamical friction before tidal disruption completely destroyed it.

The discovery of Antaeus opens many exciting possibilities for follow-up studies. A first step would be finding other members of the structure in Gaia with the information we now possess. Creating an *N*-body model for the infall of the progenitor dwarf galaxy in the potential well of the MW and exploring the possibilities for its survival in the disk would also be highly informative. Finally, it would be very helpful to measure the metallicity of more stars of our selection in order to facilitate discussions regarding the origin of the structure, and links to Sequoia in particular.

The authors thank the anonymous referee for insightful comments, and acknowledge funding from the European Research Council (ERC) under the European Unions Horizon 2020 research and innovation program (grant agreement No. 834148) and from the Agence Nationale de la Recherche (ANR projects ANR-18-CE31-0006, ANR-18-CE31-0017, and ANR-19-CE31-0017). This work has made use of data from the European Space Agency (ESA) mission Gaia (https://www.cosmos.esa.int/gaia), processed by the Gaia Data Processing and Analysis Consortium (DPAC; https://www.cosmos.esa.int/web/gaia/dpac/consortium). Funding for the DPAC has been provided by national institutions, in particular the institutions participating in the Gaia Multilateral Agreement.

Data Availability

The data used in this contribution is available in Table 1 and at doi:10.5281/zenodo.6912366.

ORCID iDs

Wassim Tenachi https://orcid.org/0000-0001-8392-3836
Rodrigo Ibata https://orcid.org/0000-0002-3292-9709
Benoit Famaey https://orcid.org/0000-0003-3180-9825
Nicolas Martin https://orcid.org/0000-0002-1349-202X

References

Amarante, J. A. S., Debattista, V. P., Beraldo e Silva, L., Laporte, C. F. P., & Deg, N. 2022, arXiv:2204.12187
Anders, F., Khalatyan, A., Queiroz, A. B. A., et al. 2022, A&A, 658, A91
Belokurov, V., Erkal, D., Evans, N. W., Koposov, S. E., & Deason, A. J. 2018, MNRAS, 478, 611
Bovy, J. 2015, ApJS, 216, 29
Bovy, J. 2020, arXiv:2012.02169
Bressan, A., Marigo, P., Girardi, L., et al. 2012, MNRAS, 427, 127
Carollo, D., Beers, T. C., Lee, Y. S., et al. 2007, Natur, 450, 1020
Collaboration, Gaia, Prusti, T., de Bruijne, J. H., et al. 2016, A&A, 595, A1
Di Matteo, P., Haywood, M., Lehnert, M. D., et al. 2019, A&A, 632, A4
Dodd, E., Callingham, T. M., Helmi, A., et al. 2022, arXiv:2206.11248
Gaia Collaboration 2022, arXiv:2206.11248
Helmi, A., Babusiaux, C., Koppelman, H. H., et al. 2018, Natur, 563, 85
Helmi, A., & de Zeeuw, P. T. 2000, MNRAS, 319, 657
Helmi, A., Veljanoski, J., Breddels, M. A., Tian, H., & Sales, L. V. 2017, A&A, 598, A58
Ibata, R., Malhan, K., Martin, N., et al. 2021, ApJ, 914, 123
Kirby, E. N., Cohen, J. G., Guhathakurta, P., et al. 2013, ApJ, 779, 102
Majewski, S. R., Nidever, D. L., Smith, V. V., et al. 2012, ApJL, 747, L37
Malhan, K., Ibata, R. A., & Martin, N. F. 2018, MNRAS, 481, 3442
Malhan, K., Ibata, R. A., Sharma, S., et al. 2022, ApJ, 926, 107
McMillan, P. J. 2017, MNRAS, 465, 76
Myeong, G. C., Evans, N. W., Belokurov, V., Sanders, J. L., & Koposov, S. E. 2018, MNRAS, 478, 5449
Myeong, G. C., Vasiliev, E., Iorio, G., Evans, N. W., & Belokurov, V. 2019, MNRAS, 488, 1235
Naidu, R. P., Conroy, C., Bonaca, A., et al. 2020, ApJ, 901, 48
Recio-Blanco, A., de Laverny, P., Palicio, P. A., et al. 2022, arXiv:2206.05541
Robin, A. C., Luri, X., Reylé, C., et al. 2012, A&A, 543, A100
Ruiz-Lara, T., Matsuno, T., Sofie Lövdal, S., et al. 2022, arXiv:2201.02405
Schönrich, R., Binney, J., & Dehnen, W. 2010, MNRAS, 403, 1829
Sestito, F., Buck, T., Starkenburg, E., et al. 2021, MNRAS, 500, 3750
Vasiliev, E. 2019, MNRAS, 482, 1525
Wang, C., Huang, Y., Yuan, H., et al. 2022, ApJS, 259, 51
Widmark, A., de Salas, P. F., & Monari, G. 2021, A&A, 646, A67
Yuan, Z., Myeong, G. C., Beers, T. C., et al. 2020, ApJ, 891, 39